Available online at www.sciencedirect.com
ScienceDirect
European Polymer Journal 43 (2007) 4662–4674
EUROPEAN POLYMER JOURNAL
www.elsevier.com/locate/europolj

Morphology and structure of poly(*p*-dioxanone)

Sebastià Gestí, Bernard Lotz [1], María Teresa Casas, Carlos Alemán, Jordi Puiggali *

Departament d'Enginyeria Química, ETS d'Enginyeria Industrial, Universitat Politècnica de Catalunya, Diagonal 647, Barcelona E-08028, Spain

Received 19 June 2007; received in revised form 13 July 2007; accepted 6 August 2007
Available online 19 August 2007

Abstract

The morphology of solution grown single crystals of poly(*p*-dioxanone) was investigated. Different crystallization conditions (solvent, precipitant agent and temperature) were tested. Dendritic growth, screw dislocations and striations were observed. Crystals usually exhibited a lozenge morphology, whose apex angle changed with the crystallization conditions. In all cases, however, a single crystal electron diffraction pattern was recorded. Spherulitic morphologies were obtained by evaporation of formic acid solutions. Lamellae gave rise to well resolved electron diffraction patterns that allowed determination of the main packing characteristics. Patterns of tilted specimens helped establish an orthorhombic unit cell, whose parameters indicate a deviation from the all *trans* molecular conformation. Quantum mechanical calculations were performed on small model compounds to study the conformational preferences. Simulated diffraction patterns were consistent with a unit cell containing four repeat units and a $P2_12_12_1$ space group. Molecular packing suggests the existence of different kinds of folds for an assumed adjacent reentry. Polyethylene decoration hardly highlighted a crystal sectorization. Also enzymatic degradation of lamellar crystals was evaluated by using a *Pseudomonas cepacia* lipase.

Keywords: Crystal morphology; Lamella; Electron microscopy; Poly(*p*-dioxanone); Molecular conformation

1. Introduction

Poly(*p*-dioxanone) (PPDX or PPDO) is a synthetic poly(ester–ether) that attracts increasing interest for biomedical applications due to its biodegradability, biocompatibility, bioabsorbability, softness and flexibility [1]. It was patented [2] in 1977 as an absorbable polymer and processed as a monofilament surgical suture in the early 1980s [3]. Since then, the polymer has been commercialized under different tradenames (PDS by Ethicon Inc. and Monoplus by B. BRAUN).

The chemical repeat of the polymer is $-[CH_2-CH_2-O-CH_2-CO-O]_n-$. The ether bond and the additional methylene groups provide greater flexibility than polyglycolide, which is the most common material used as a bioabsorbable surgical suture.

PPDX can also be injection-molded. This gives rise to other biomedical applications such as bone or tissue fixation devices [4], fasteners and drug delivery systems [5]. The crystallization kinetics and spherulite morphology of PPDX have been

* Corresponding author. Tel.: +34 93 401 66 84; fax: +34 93 401 71 50.
E-mail address: Jordi.Puiggali@upc.es (J. Puiggali).
[1] Permanent address: Institut Charles Sadron (CNRS-ULP), 6 rue Boussingault, 67083 Strasbourg, France.

0014-3057/$ - see front matter © 2007 Elsevier Ltd. All rights reserved.
doi:10.1016/j.eurpolymj.2007.08.007

extensively studied with polarized optical microscopy [6], differential scanning microscopy [7], synchrotron small-angle X-ray scattering [8], dielectric relaxation spectroscopy [9] or hot-stage optical microscopy [10]. Influence of degradation on morphology, properties and crystallization kinetics have been also widely studied for PPDX [11–14] and also for diblock copolymers of PPDX and poly(ε-caprolactone) [15–17]. Surprisingly, the single crystal morphology and crystalline structure of PPDX are less well studied. An orthorhombic unit cell containing two molecular segments and a $P2_12_12_1$ space group has recently been reported, based on electron and X-ray diffraction data [18]. This kind of unit cell was assigned by considering a meridional reflection observed in tilted X-ray fiber diffraction patterns and indexed as 002. The suggested unit cell dimensions would imply a molecular conformation with a tight pitch since a 52% shortening of a zig-zag conformation was deduced.

Preliminary morphological studies showing different crystalline habits have been performed by different authors [6,10,19]. Significant changes with temperature have been reported. Spherulites obtained at temperatures higher than 90 °C were double-ringed [6] and did not show the characteristic Maltese cross [10]. This kind of spherulites is characteristic of materials that possess a biaxial indicatrix twisted about the optic normal, which is aligned parallel to the spherulitic radius, and thus is consistent with a low symmetry unit cell (orthorhombic or lower). Spherulites obtained at lower temperatures (<75 °C) exhibited the characteristic Maltese cross and a single extinction pattern. Spherulites showing both features could be obtained when crystallization was carried out in two steps at high and low temperature. Although no change in the crystalline structure could be detected by X-ray diffraction studies [6]. Kinetic crystallization studies [6] suggested two different crystallization regimes (III and II) with a transition in the range of 75–80 °C.

In the present work, we study further the crystalline structure and the crystalline morphology of both single crystals and spherulites of poly(*p*-dioxanone).

2. Experimental section

Poly(*p*-dioxanone) sutures were purchased from Ethicon. Samples were undied by exposition to chloroform before conducting the structural studies.

Lamellar crystals of poly(*p*-dioxanone) were obtained by isothermal precipitation. Drops of precipitants such as *n*-butanol, 2-methyl-2,4-pentanediol or 2,5-hexanediol were added to dilute formic acid or hexafluoroisopropanol solutions (0.25–1 mg/mL) at temperatures between 40 and 60 °C. In all cases, crystals were recovered from mother liquor by centrifugation, repeatedly washed with *n*-butanol and deposited on carbon-coated grids. As an alternative method, single crystals were also prepared on mica at room temperature by evaporation of a dilute solution (0.015 mg/mL) in a mixture of formic acid/*n*-butanol (1/4 v/v). Crystals were coated with a thin carbon film which was then floated off on water. Grids of the different preparations were shadowed with Pt–Carbon at an angle of 15° for bright field observations. Polymer decoration was achieved by evaporating polyethylene onto the surface of single crystals, as described by Wittmann and Lotz [20].

Spherulites were prepared by slow evaporation between two cover-slips of a drop of a formic acid solution (polymer concentration 5%). The spherulites were coated with a thin carbon film, floated off on water and picked up on copper grids for electron microscopy observations.

Degradation of single crystals was performed with a *Pseudomona cepacia* lipase (40 units/mg). Lamellar crystals were deposited on carbon-coated gold grids which were immersed on 20 μL of a pH 7.0 buffered medium of 50 mM Tris–HCl containing the enzyme (0.13 mg/mL) and maintained at 37 °C. After different exposure times the grids were repeatedly washed with distilled water and ethanol, and shadowed with Pt–Carbon. Controls without enzyme were also run.

Optical photographs were taken with an Olympus Camedia C-3040 digital camera mounted on an Olympus BX51 microscope.

Philips TECNAI 10 and CM12 electron microscopes were used and operated at 80 and 100 kV for bright field and electron diffraction modes, respectively. *hk*0 and tilted electron diffraction patterns were recorded on Kodak Tri-X films and with a Megaview III digital camera from Soft Image System (SIS), respectively. The patterns were internally calibrated with gold ($d_{111} = 0.235$ nm).

AFM examination of single crystals was performed with Digital Instruments Nanoscope IV under tapping mode using silicon tips with a 25 kHz resonance frequency and a 0.4 N/m spring constant. Height and amplitude images were recorded simultaneously.

X-ray fiber patterns were obtained under vacuum at room temperature, using calcite as a calibration standard. A modified Statton camera (W.R. Warhus, Wilmington, DE, USA) with Ni-filtered copper radiation ($\lambda = 0.1542$ nm) was used. The X-ray beam was directed perpendicular to the stretching direction for films and fibers. Fibers were prepared from the melt and annealed under stress at 50 °C. Quantum mechanical calculations were carried out with the Gaussian 03 computer program [21]. Conformational analyses of two model compounds were performed by Density Functional Theory (DFT) calculations with the following combination: the Becke's three-parameter hybrid functional (B3) [22] and the Lee, Yang and Parr (LYP) [23] expression for the nonlocal correlation (B3LYP). The 6-31 + G(d,p) basis set [24] was used in all calculations, which were run on the "Centre de Supercomputació de Catalunya".

Structural modeling was carried out with the diffraction software package of the Cerius^2 computer program (Accelrys Inc.) [25]. All calculations were run on a Silicon Graphics Octane Workstation.

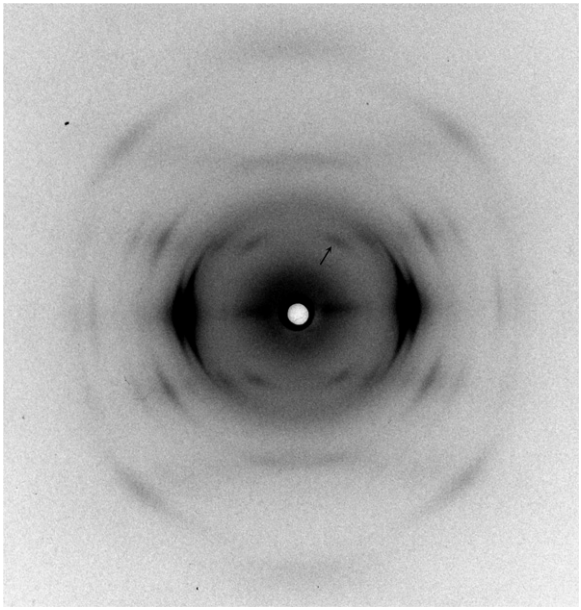

Fig. 1. X-ray fiber diffraction pattern of poly(*p*-dioxanone). Arrow indicates the strong reflection observed on the first layer line at 0.539 nm.

3. Results and discussion

3.1. Unit cell determination using tilted electron diffraction patterns

X-ray fiber diffraction patterns of poly(*p*-dioxanone) are characterized by well defined equatorial reflections, and by broad diffuse non equatorial spots extending over three layer lines (Fig. 1). Patterns have recently been indexed according to an orthorhombic unit cell with $a = 0.970$ nm, $b = 0.742$ nm, $c = 0.682$ nm. However, this cell geometry must be considered as tentative. Indeed, several overlappings of reflections were assumed to account for the measured spacings [18] (e.g., the observed spot at 0.529–0.539 nm was attributed to the 1 0 1 and 0 1 1 reflections whose theoretical spacings were 0.558 and 0.502 nm, respectively). Furthermore, patterns obtained with the X-ray beam perpendicular to the fiber direction did not show any meridional reflections that could clearly indicate that the unit cell is orthorhombic. In fact, only a reflection indexed as 0 0 2 was observed on the meridian when the fiber was tilted by approximately 15°. On this basis a 2_1 molecular symmetry was deduced, indicating a significant shortening of the repeat unit compared to the all *trans* conformation (monomer lengths of 0.34 nm and 0.73 nm, respectively). This feature suggested that poly(*p*-dioxanone) has an unusual molecular conformation.

An alternative, but, as it turns out, ultimately incorrect indexing of the fiber pattern could consider a monoclinic unit cell with $a = 1.149$ nm, $b = 0.74$ nm, $c = 0.634$ nm and $\beta = 112.5°$. Thus, the strong spot on the first layer line at 0.539 nm would be the 0 0 1. A lower molecular symmetry, and a more limited chain axis shortening could be expected. Analysis of electron diffraction patterns from lamellar crystals (described in the next section) at different tilting angles is an adequate, complementary tool to elucidate the cell parameters of poly(*p*-dioxanone). Electron diffraction patterns obtained from large pyramidal crystals always had a *2mm* symmetry when tilting around both the a^* (Fig. 2) and b^* (Fig. 3) reciprocal axes. Furthermore, the sense of the tilt did not affect the diffraction pattern. Thus, an orthorhombic space group can be assumed rather than a monoclinic cell with the α or β angles different from 90°. A large fraction of the reciprocal space was explored since patterns could be easily obtained for tilting angles up to 50–60°. Spots are well defined and yield accurate spacing data. Table 1 summarizes the observed reflections and indexing according to an orthorhombic unit cell with $a = 0.970$ nm, $b = 0.751$ nm, $c = 0.650$ nm,

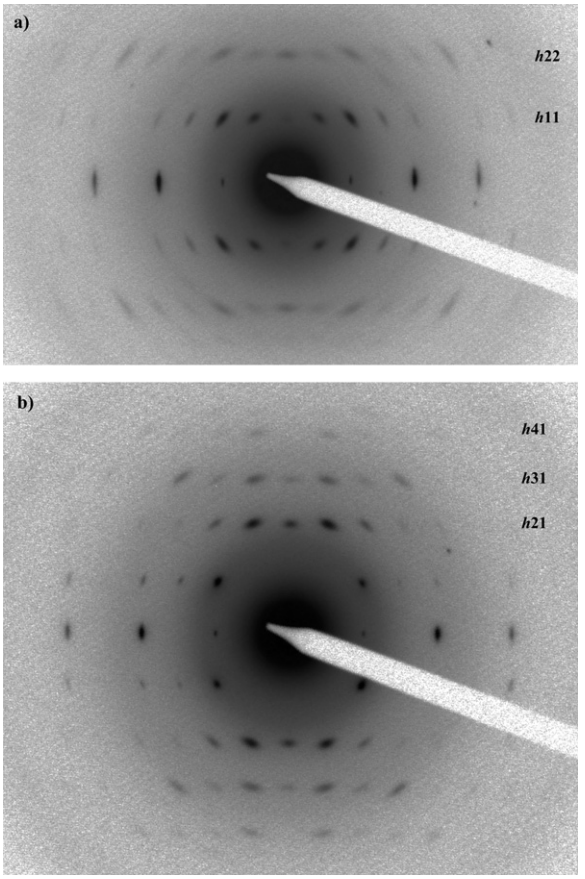

Fig. 2. Electron diffraction patterns of lamellae tilted around the a^* axis by 50° (a) and 28° (b). Reflections corresponding to the $h11$ and $h22$ layer lines are present in (a), $h31$ spots are present in (b). In the latter case reflections of $h21$ and $h41$ layers can also be seen; they are however weaker than expected, since they are not exactly on the Ewald sphere.

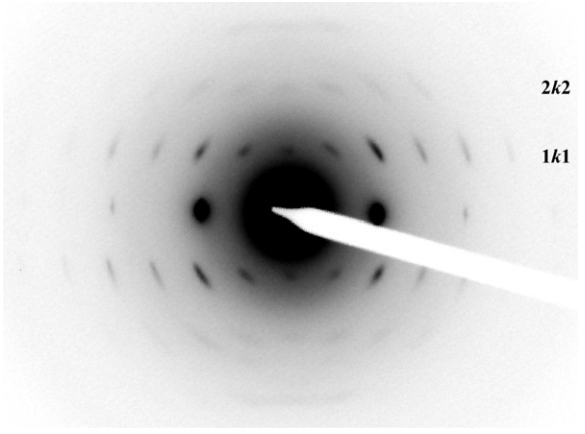

Fig. 3. Electron diffraction pattern of a lamellar crystal tilted around the b^* axis by 60° displaying the $1k1$ reflections.

Table 1
Calculated and measured X-ray and electron diffraction spacings d (nm) for poly(*p*-dioxanone)

$h\ k\ l$[a]	d_{calcd}	d_{measd}[b]	d_{measd}[c]
1 1 0	0.594	0.595 w E	
2 0 0	0.485		0.484 w
2 1 0	0.407	0.407 vs E	
0 2 0	0.376	0.376 vs E	0.376 vs
1 2 0	0.350	0.349 w E	
4 0 0	0.243	0.243 m E	0.243 s
4 1 0	0.231	0.230 w E	
0 4 0	0.188		0.188 vw
6 0 0	0.162		0.162 m
1 0 1	0.540	0.539 s off M	0.537 vs
0 1 1	0.491		0.492 w
1 1 1	0.438	0.438 s off M	0.438 s
2 1 1	0.345	0.344 w off M	0.344 vs
0 2 1	0.325		0.326 vs
1 2 1	0.308	0.308 s off M	0.309 vs
3 0 1	0.289	0.289 w off M	
3 1 1	0.270	0.269 m off M	0.270 s
2 2 1	0.270		0.270 s
0 3 1	0.234	0.229 w off M	0.233 m
3 2 1	0.229		0.229 w
1 3 1	0.227	0.227 w off M	0.227 s
4 1 1	0.217		0.217 m
2 3 1	0.210		0.211 w
4 2 1	0.194		0.195 vw
3 3 1	0.189		0.189 s
1 4 1	0.177		0.177 m
6 1 1	0.154		0.154 w
1 5 1	0.145		0.145 w
1 6 1	0.122		0.123 vw
1 0 2	0.308	0.303 m off M	
2 0 2	0.270	0.269 w off M	0.271 vw
2 1 2	0.254		0.254 w
0 2 2	0.246		0.245 s
1 2 2	0.238	0.238 w off M	0.238 m
3 1 2	0.219	0.218 m off M	
2 2 2	0.219		0.218 s
3 2 2	0.196		0.194 w
2 3 2	0.184		0.183 vw
4 2 2	0.173		0.172 w
5 2 2	0.152		0.152 m
0 1 3	0.208	0.204 w off M	

[a] Indexing on the basis of an orthorhombic unit cell with $a = 0.970$ nm, $b = 0.751$ nm and $c = 0.650$ nm.

[b] From X-ray fiber diffraction patterns. Abbreviations denote relative intensities and orientations: vs, very strong; s, strong; m, medium; w, weak; M, meridional; E, equatorial; off M, off meridional.

[c] From tilted single crystal electron diffraction patterns. Abbreviations denote relative intensities: vs, very strong; s, strong; m, medium; w, weak; vw, very weak.

which is in agreement with that previously reported [18], although an even slightly greater shortening of the chain repeat is found.

3.2. Single crystals morphology

Poly(*p*-dioxanone) crystallizes as large pyramidal entities with a lozenge morphology, when a dilute solution (one volume of formic acid and four volumes of *n*-butanol) is slowly evaporated. The crystal lateral dimensions may reach 200 μm (Fig. 4a) and are ideally suited for tilting diffraction experiments. The pyramid shape results from multilayered crystal growth as shown by AFM.

A dendritic growth trend is often observed (Figs. 4b and 5) when solvent evaporation is rapid and crystal growth becomes controlled by diffusion. High molecular weight poly(*p*-dioxanone) samples form dendrites with primary, secondary and tertiary branches (Fig. 5). In the tertiary branches the thickness of individual lamellae is ~7 nm, whereas primary branches are multilayered.

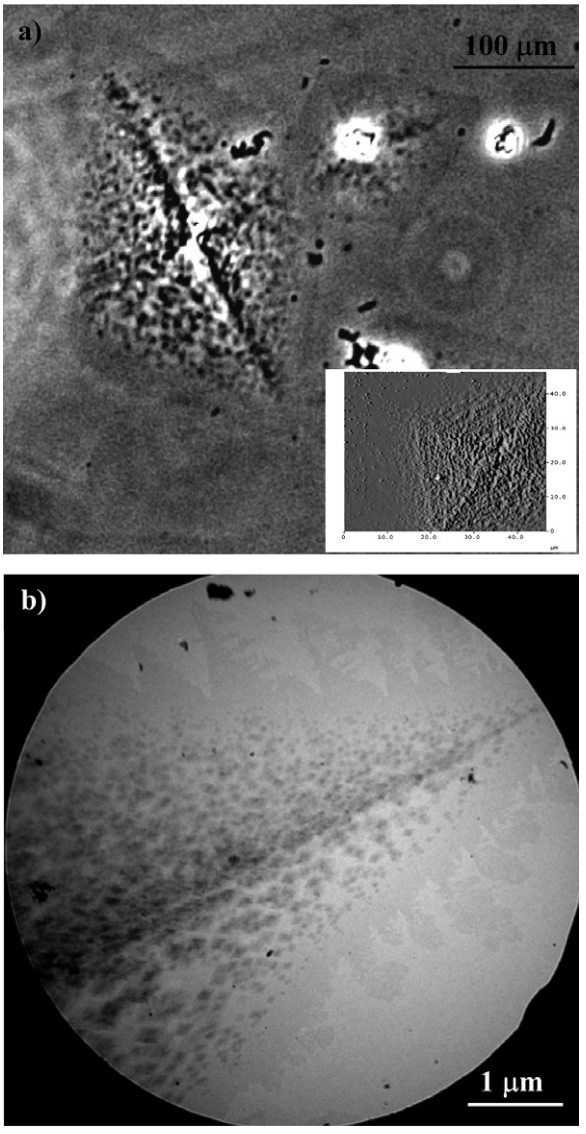

Fig. 4. (a) Phase contrast micrograph of poly(*p*-dioxanone) lozenge-shaped pyramidal crystals obtained by evaporation at room temperature of a dilute solution of formic acid/*n*-butanol (1/4 v/v). Inset shows an AFM image of a multilayered crystal. (b) Electron micrograph of poly(*p*-dioxanone) aggregates obtained under similar conditions. A large crystal with smaller lozenge overgrowths is shown. Note the dendritic habit developed in the basal lozenge crystal, which is usually associated with diffusion-controlled growth.

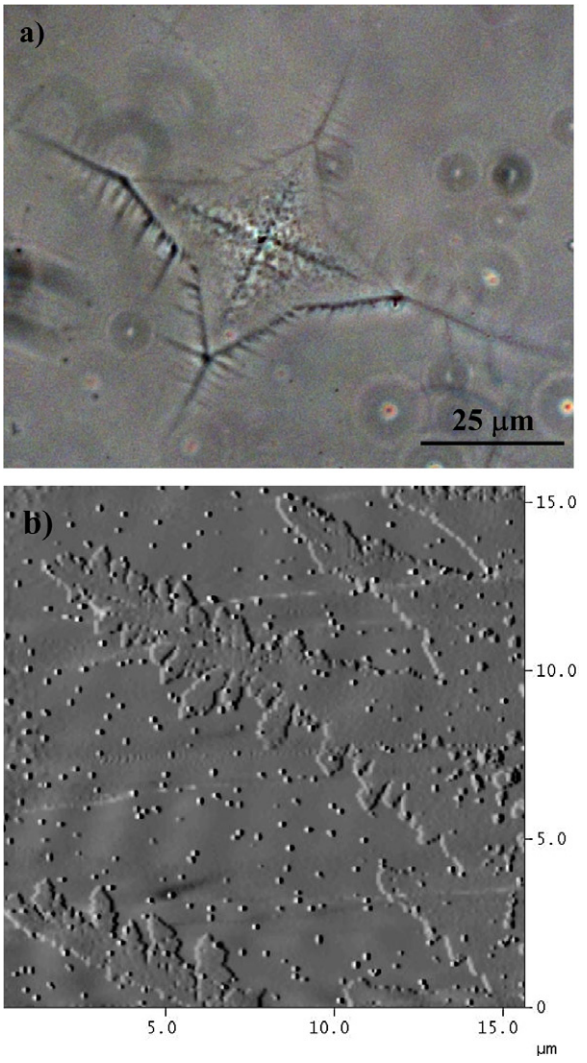

Fig. 5. (a) Phase contrast micrograph of an irregular poly(*p*-dioxanone) aggregate obtained by evaporation of a 1/4 v/v formic acid/*n*-butanol solution at room temperature. Note the dendritic growth occurring at the crystal corners. (b) AFM image showing the hyperbranched structure.

Flat lamellar crystals with lozenge shape morphologies are produced in a dilute formic acid solution with four volumes of butanol at 40 °C (Fig. 6a). The growth faces are up to 8 μm wide. In addition, smaller screw dislocations of different handness develop on these crystals. The relative orientation of selected area electron diffraction patterns and bright field (Fig. 6b) indicates that the crystals are bound by four {1 1 0} faces, which form angles of 103–107° and 72–77° (compared to 105° and 75° calculated from the unit cell dimensions). The long diagonal of the lozenges is the reciprocal a^* axis.

Diffraction patterns indicate that molecular chains are perpendicular to the crystal basal plane, which implies chain folding considering the molecular weight of the polymers and the lamellar thickness of only 7 nm.

$hk0$ electron diffraction patterns display many reflections (Table 2), a *2mm* symmetry and $0k0$ systematic absences for odd k values. Both the high and low intensities of the 2 1 0 and 1 1 0 reflections, respectively, are worth emphasizing since they clearly suggest that the unit cell contains four

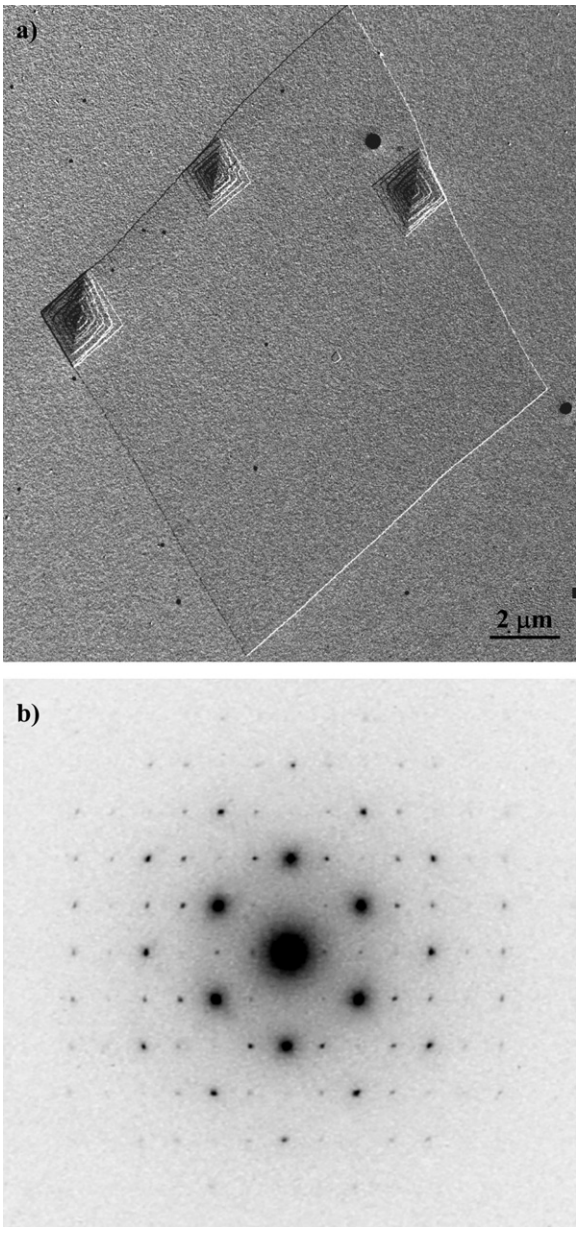

Fig. 6. (a) Electron micrograph of a single lamella with some small terrace growths of poly(*p*-dioxanone) obtained by adding four volumes of butanol to a dilute formic acid solution (1 mg/mL) at 40 °C. (b) Corresponding $hk0$ electron diffraction pattern.

Table 2
Calculated and measured electron diffraction spacings d (nm) for poly(*p*-dioxanone) single crystals

$h\ k\ l$[a]	d_{calc}	d_{measd}[b]
1 1 0	0.594	0.594 vw
2 0 0	0.485	0.484 w
2 1 0	0.407	0.407 vs
0 2 0	0.376	0.376 vs
1 2 0	0.350	0.349 m
2 2 0	0.297	0.297 vw
3 1 0	0.297	0.297 m
3 2 0	0.245	0.245 m
4 0 0	0.243	0.243 s
1 3 0	0.242	0.243 vw
4 1 0	0.231	0.231 w
2 3 0	0.222	0.221 s
4 2 0	0.204	0.204 s
3 3 0	0.198	0.198 w
5 0 0	0.194	0.193 vw
0 4 0	0.188	0.188 m
5 1 0	0.188	0.188 vw
1 4 0	0.184	0.184 vw
2 4 0	0.175	0.175 vw
4 3 0	0.174	0.174 vw
5 2 0	0.172	0.173 vw
3 4 0	0.162	0.162 vw
6 0 0	0.162	0.162 w
6 1 0	0.158	0.158 w
5 3 0	0.153	0.153 vw
4 4 0	0.148	0.148 vw
6 2 0	0.148	0.148 vw
1 5 0	0.148	0.148 vw
2 5 0	0.143	0.143 vw
3 5 0	0.136	0.136 vw
6 3 0	0.136	0.136 vw
0 6 0	0.125	0.125 vw

[a] Indexing on the basis of orthorhombic unit cell with $a = 0.970$ nm, $b = 0.751$ nm and $c = 0.650$ nm.

[b] Abbreviations denote relative intensities: vs, very strong; s, strong; m, medium; w, weak; vw, very weak.

molecular segments instead of only two, as reported previously. This observation and the experimental density (1.38 g/cm^3) [18] suggest that the chain axis repeat distance (0.650 nm) is spanned by only one residue. Thus the calculated density becomes 1.43 g/cm^3, which is very close to the observed value. Patterns also show weak 100, 300 and 500 reflections that should be absent for a $P2_12_12_1$ space group, but may arise from dynamic scattering effects. The latter cannot be fully discarded in spite of the limited thickness of the lamellae.

Single crystals of poly(*p*-dioxanone) also show some additional features when observed at high magnification. In particular they display essentially continuous striations running outwards from the center of the crystal (Fig. 7a). The angle formed between the striations and the corresponding growth faces may differ from 90°. Similar striations have been reported for different polyesters (e.g., polyester 4 6 [26], polyester 12 10 [27], poly-β-propiolactone [28] and poly-ε-caprolactone [29]). Their origin is still unclear and has been attributed variously to the existence of different chain-packing states in the crystal, a twinning involving a small chain axis shear of molecular chains, or an aggregation of microcrystals.

The lozenge crystals become more squared when precipitation takes place at higher temperatures, as shown by the spiral growths in Figs. 7b and 8a, the latter grown around 60 °C and with precipitant 2-methyl-pentanediol or 1,6-hexanediol. The acute angle increases to ~82°, which corresponds to the angle between the {320} faces. Actually the changes in morphology overtake the square habit, which means that the reciprocal a^* axis becomes parallel to the short rather than the long diagonal of the lozenge, as expected for {320} growth faces.

Similar changes in the apex angle with crystallization temperature have been reported for poly-(3,3-bis(chloromethyl)oxacyclobutane) (PBCMO) crystals [30–32], and were explained in terms of different chain folding modes. Fold planes varied from {110} to {210}, in which case a complex distribution requiring alternation of two kinds of folds (if adjacent reentry is postulated) [30]. A related explanation based on a combination of different folds can be given for poly(*p*-dioxanone) to justify both {110} and {320} folding planes, as discussed below.

Crystals formed at high temperature display curved growth faces. The large basal crystals that are first formed in the crystalline aggregates of

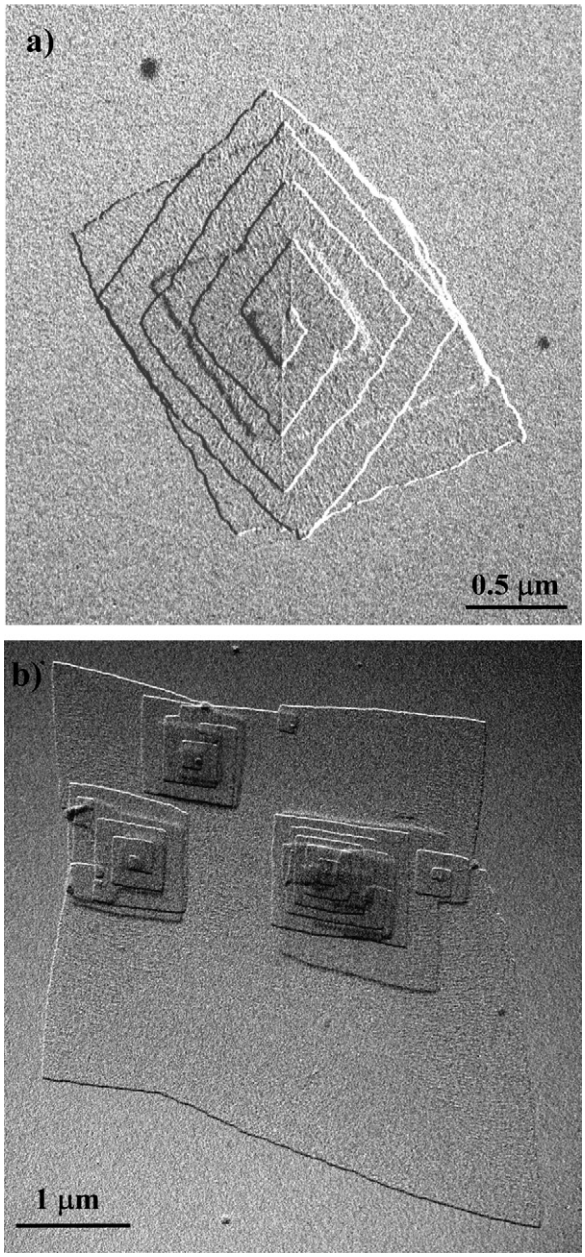

Fig. 7. Electron micrographs of poly(*p*-dioxanone) lamellar crystals prepared as in Fig. 6 at 40 °C (a) and 50 °C (b). (a) Lozenge lamella with spiral growths and noticeable striation. A second spiral growth crystal can also be seen. (b) Irregular crystal with different screw dislocation overgrowths. Note that the small crystals tend to display a square morphology.

poly(*p*-dioxanone) shown in Fig. 8b clearly reveal a lenticular morphology. Also, multiple helical overgrowths with square morphology subsequently are formed. This feature, already observed in polyethylene [33–37] has been interpreted as a result of

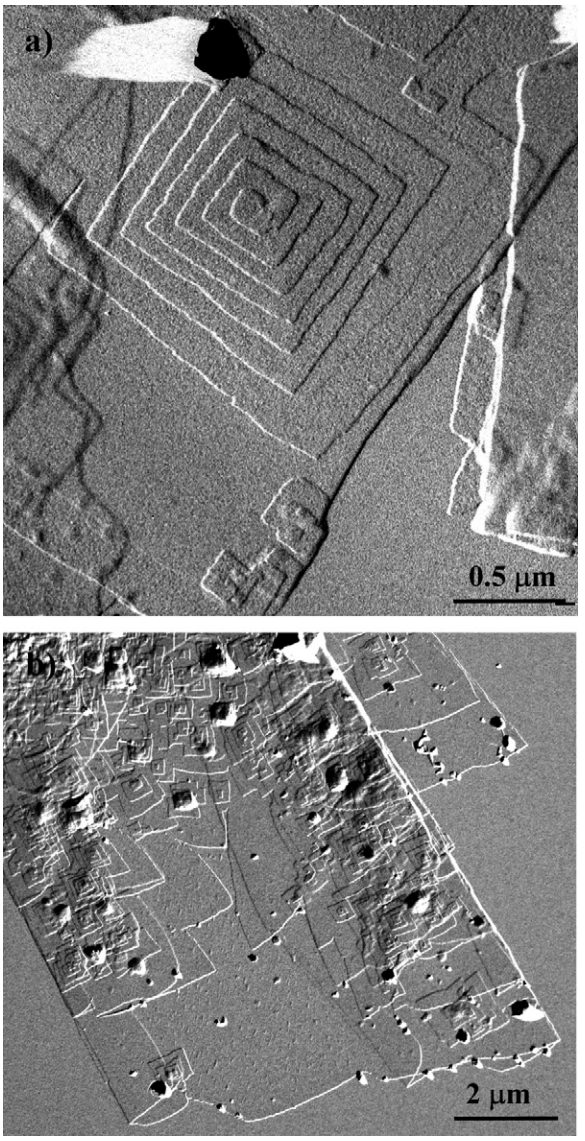

Fig. 8. Electron micrographs of poly(*p*-dioxanone) lamellar crystals prepared by precipitation with 2-methyl-2,4-pentanediol of a dilute polymer solution in formic acid at 60 °C. (a) Spiral growth of nearly square lamellae and (b) crystal aggregates with spiral overgrowths and some lanceolate morphologies.

growth intermediate between nucleated and rough-surface type.

Polyethylene decoration hardly highlighted a sectorization of single crystals caused by a regular folding mechanism (i.e., Fig. 9). Decorating rods were nevertheless preferably oriented perpendicular to the growth faces, suggesting that some chain folds or loops are parallel to the growth faces.

Single crystals of poly(*p*-dioxanone) could be degraded easily by exposition to enzymatic attack.

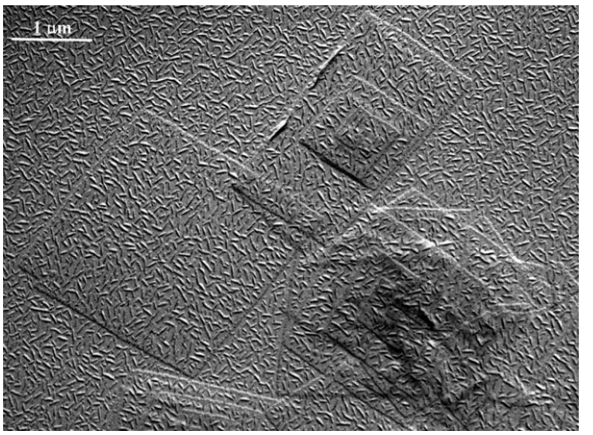

Fig. 9. Polyethylene decoration of poly(*p*-dioxanone) lamellar crystals obtained by adding four volumes of *n*-butanol to a dilute polymer solution in hexafluoroisopropanol (0.25 mg/mL) at 55 °C.

The attack of the *Pseudomonas cepacia* lipase was similar for the four growth faces of the crystals. At short exposure times (Fig. 10a) only the smaller lamella showed serrated edges indicative of the enzymatic attack, but after 45 min serration was observed even in the large basal crystals (Fig. 10b). In the process the small overgrown crystal became rounded as a consequence of the disappearance of the initial edges. It is also clear that degradation was initiated at the edges of the lamellar crystals: no holes were detected on their surfaces. Such holes have been reported during degradation of various polyesters and have been interpreted as an attack limited to the loose loops existing in the surface [38,39].

3.3. Spherulites from solvent evaporation

Evaporation at room temperature of a 5% polymer solution in formic acid yields well developed spherulites. They contrast with the lamellar crystals observed upon evaporation of more dilute solutions in mixtures of formic acid and butanol. Spherulites have diameters up to 200 μm and show well defined and regularly spaced rings in their inner part (Fig. 11a). A fibrillar texture is observed in the outer parts corresponding to faster crystallization of more concentrated polymer solutions. Rings progressively become diffuse along the spherulite radius and disappear with the development of the fibrillar texture.

In terms of optical properties, all the observed spherulites are characterized by the typical Maltese

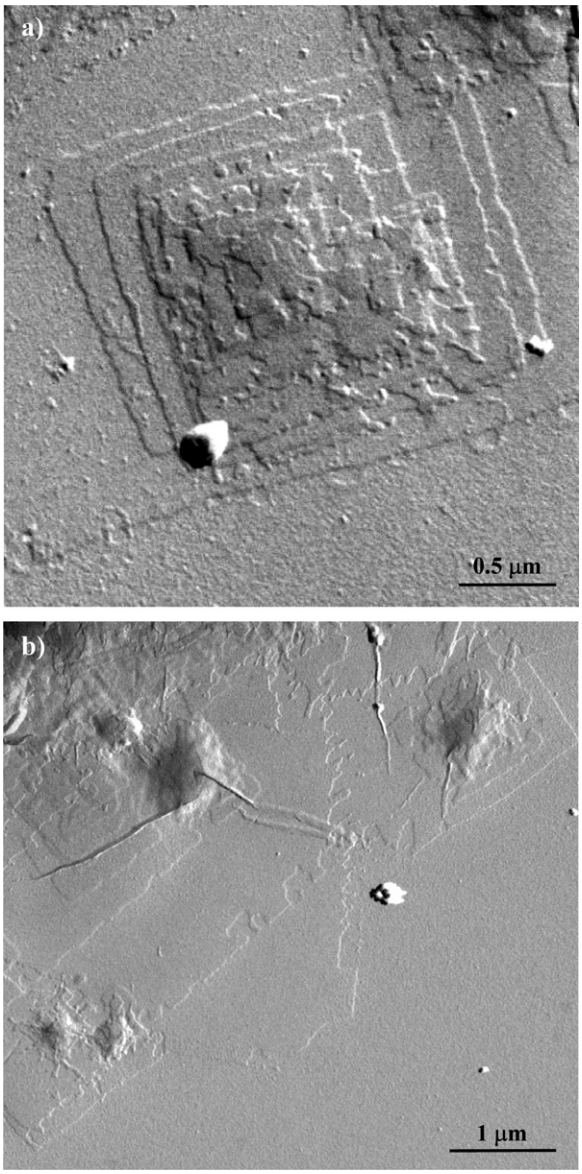

Fig. 10. Electron micrographs of poly(*p*-dioxanone) lamellar crystals obtained from a 1,6-hexanediol/formic acid mixture and exposed to a *Pseudomonas cepacia* lipase medium at 37 °C for 15 min (a) and 45 min (b).

cross and a negative birefringence. These solution grown spherulites are similar to the single-banded ones produced by crystallization from the melt at temperatures lower than 75 °C.

The thin spherulites obtained by solvent evaporation are suitable for electron microscopy observation as shown in Fig. 11b. The central part shows again a ringed texture with spacing ~3 μm. Black rings correspond to the thicker areas associated with twisted lamellae when the latter are edge-on.

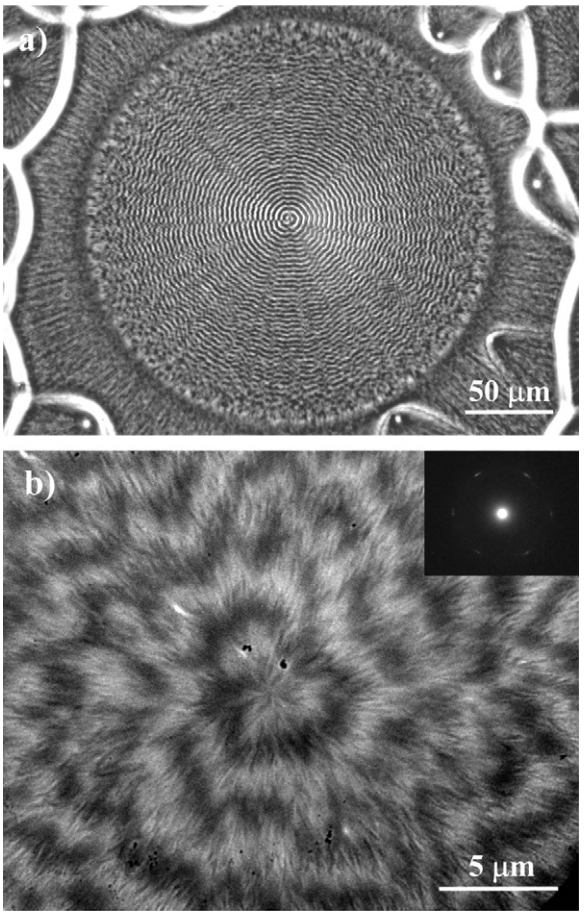

Fig. 11. (a) Phase contrast optical micrograph of a poly(*p*-dioxanone) spherulite prepared by slow evaporation at room temperature of a 5% polymer solution in formic acid. (b) Electron micrograph of the inner part of a spherulite obtained by evaporation. Inset shows the corresponding electron diffraction pattern.

*hk*0 electron diffraction patterns, from the thinner zones, are similar to those previously reported for solution crystallized single crystals. They further indicate that the a^* axis is parallel to the spherulite radius.

3.4. Molecular conformation

In order to approach the structure of poly(*p*-dioxanone), the conformational preferences of a short analog, CH_3–COO–$(CH_2)_2$–O–CH_2–COO–CH_3 (**I**) were investigated by DFT calculations. As this model compound has possible rotations around five bonds and each one is expected to have three minima (i.e., *gauche*$^+$ (60°), *trans* (180°) and *gauche*$^-$ (−60°)), $3^5 = 243$ minima should be

considered for the potential energy surface of I, assuming that the two ester bonds have *trans* arrangement. However, as we are only interested in conformations that match the observed monomer length (0.65 nm), only structures with one or two folded dihedral angles were considered. Furthermore, due to the absence of chiral atoms and the symmetry of the molecule the number of conformations to be optimized is significantly reduced. Accordingly, only 25 initial structures were considered for complete geometry optimizations at the B3LYP/6-31 + G(d,p) level. These were five structures with one folded dihedral angle (g^+) and 20 structures with two folded dihedral angles (10 with the two dihedral angles in g^+ and 10 with one dihedral angle in g^+ and the other in g^-). Furthermore, in order to evaluate the tendency of **I** to adopt partially folded conformations, the fully-extended conformation (with all dihedral angles in *trans*) was added to the cast of initial structures.

Geometry optimization led to 20 different minimum energy conformations. Fig. 12 represents the energy relative to the optimized fully-extended conformation of each minimum against the corresponding monomer length. It appears that 10 of the optimized structures are more stable than the fully-extended one. Four of these minima have energy lower by at least 1.5 kcal/mol. These results show that **I** has a significant tendency to adopt folded arrangements. In addition the monomer length of the lowest energy conformation (**Ia**) is 0.651 nm, in excellent agreement with experimental observations. The monomer length of the next three minima (with 0.5 (**Ib**), 0.6 (**Ic**) and 0.6 (**Id**) kcal/mol higher energies) are 0.660, 0.604 and 0.620 nm, respectively. The dihedral angles of these structures are listed in Table 3. The four minima show a common conformational pattern: the dihedral angle $CH_2O–CH_2CO$ adopts a folded arrangement in all cases.

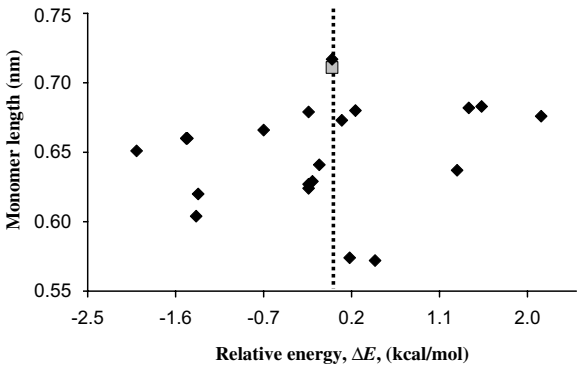

Fig. 12. Representation of the monomer length of the minima calculated for **I** against their energy relative to that of the fully-extended conformation. The square symbol indicates the optimized fully-extended conformation. Note that the corresponding length is shorter than the theoretical value of 0.73 nm.

In order to check if the ranking of low energy conformations displayed in Table 1 changes with the molecular length, additional calculations were performed on a model compound with two monomers: $CH_3–CO(O–(CH_2)_2–O–CH_2–CO)_2O–CH_3$ (**II**), and starting with the minimum energy conformations listed in Table 1. Two different cases were examined: (i) the dihedral angles of the two monomers were set at identical values, and (ii) the dihedral angles of the two monomers were equal but with opposite sign. Accordingly, eight structures were considered in the conformational study of **II**. After B3LYP/6-31 + G(d,p) optimizations, and imposing that the dihedral angles of the two monomers are identical, we found that the conformation derived from **Ia** is more stable than the other ones by at least 1.3 kcal/mol. Interestingly, the second minimum was that derived from **Ia** but considering opposite signs in the dihedral angles of the two monomers.

A survey of the Cambridge Structural Data Base [40] did not show any crystal structures with exact representative fragments of the polymer unit repeat. However, seven crystal structures containing similar acyclic $CH_2OCH_2CH_2OCH_2COO$ fragments were found. In general, the ethylene glycol and the glycolic acid residues tend to adopt the postulated TGT and $\overline{G}T$ conformations, respectively. Unit cells usually show a center of inversion, and consequently these fragments exist also with opposite signs for the indicated dihedral angles. The exact theoretical conformation has been found for three compounds in which the studied fragment

Table 3
Dihedral angles[a] (in deg), monomer length (*d*, in nm) and relative energy (ΔE, in kcal/mol) of the low energy minima calculated for **I** at the B3LYP/6-31 + G(d,p) level

Structure	φ_1	φ_2	φ_3	φ_4	φ_5	*d*	ΔE
Ia	177.9	−71.4	170.5	74.1	173.9	0.651	0.0
Ib	178.4	−178.6	176.8	75.4	176.3	0.660	0.5
Ic	179.8	71.7	171.6	74.3	179.9	0.604	0.6
Id	86.6	173.9	172.5	75.2	175.8	0.620	0.6

[a] Named according to the chemical repeat unit shown in Scheme 1 that shows the dihedral angles adopted in the proposed structure.

corresponds to lateral groups of cyclic compounds (NUNSUK [41], RISSIV [42] and RISTAO [42]). In addition, the TGT (or T$\overline{G}$T) conformation for the ethylene glycol residue has been experimentally confirmed for 52 solved crystal structures in which 70% of $CH_2OCH_2CH_2OCH_2$ fragments have the indicated conformation. Acyclic CH_2OCH_2COO fragments have been found in the structures of 37 compounds. In this case, results are less clear although either a *trans* (71%) or a *gauche* (29%) conformation are observed for the first CH_2O–CH_2CO torsion angle and a *trans* conformation is clearly dominant for the second OCH_2–COO dihedral angle. Finally, it should be noted that the molecular conformation of several polyesters with ethylene glycol units has been determined. Although no clear trend emerges, a TGT conformation was assumed for one of the polymorphic forms of poly(ethylene succinate) [43,44].

3.5. Molecular packing from electron diffraction data

A preliminary model of molecular packing was built considering the molecular conformation predicted by the quantum mechanical calculations and assigning a $P2_12_12_1$ space group to the orthorhombic unit cell containing four molecular segments.

Standard bond distances and bond angles were adopted as well as the dihedral angles indicated in Scheme 1, which match the experimental repeat unit length. Note that in this model the binary screw axis parallel to the chain axis does not correspond to a molecular symmetry element. In fact, this axis links neighboring chains along the [2 1 0] crystallographic direction, as shown in Fig. 13, and results in generation of a non polar crystal structure. Note however that the molecular chain is polar since there is only one carbonyl group in the postulated chain repeat unit. Thus, the indicated symmetry axis appears as a necessary feature since it avoids a polar crystal. Furthermore, the space group leads to a structure in which all molecules have the same chirality, a feature that can reflect the preference for the TGT$\overline{G}$TT conformation deduced by quantum mechanical calculations on small compounds.

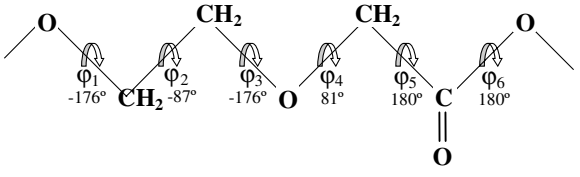

Scheme 1.

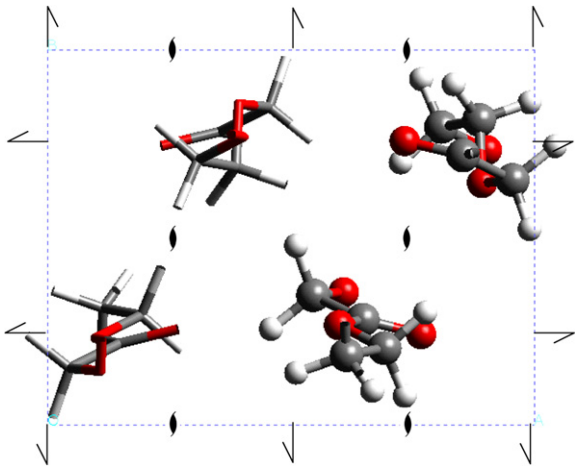

Fig. 13. View parallel to the *c*-axis direction showing the optimized packing of poly(*p*-dioxanone) whit TGT$\overline{G}$TT chain conformation, a unit cell with *a* and *b* parameters 0.970 and 0.751 nm, respectively, and a $P2_12_12_1$ space group. For clarity up and down chains are represented by sticks, and by balls and sticks, respectively. Color code: white = hydrogen; grey = carbon; red = oxygen. (For interpretation of the references in color in this figure legend, the reader is referred to the web version of this article.)

The azimuthal setting angle of one molecule (e.g. number 1 in Fig. 13) was optimized by qualitative matching of the experimental and simulated *hk*0 electron diffraction patterns. The position of the other molecules is fixed by the space group symmetry. A reasonable agreement was achieved for 75° setting angle (angle between the 0 0 1 projection of the C=O bond and the *b* axis). The electron diffraction analysis thus confirms the main features of the packing. However, it is also clear that some reflections of the simulated pattern (Fig. 14) have stronger intensity than experimentally observed (e.g., 2 2 0 and 2 4 0 reflections). Multiple scattering effects, as also indicated by the presence of weak 1 0 0 and 5 0 0 reflections, preclude an accurate analysis of the electron diffraction pattern intensities. A structural refinement implying dihedral angles and the chain axis shift between molecules should be performed against the X-ray diffraction data, but the poor quality of the available diffraction patterns makes the task difficult.

An interesting feature of the postulated packing is that there is an alternation of two neighboring chains with the same up or down orientation in

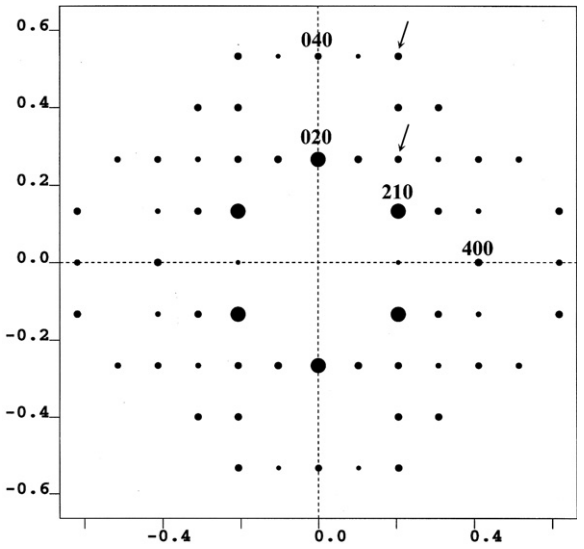

Fig. 14. Simulated $hk0$ electron diffraction pattern of poly(*p*-dioxanone) assuming the refined molecular packing shown in Fig. 13. Arrows indicate the problematic reflections.

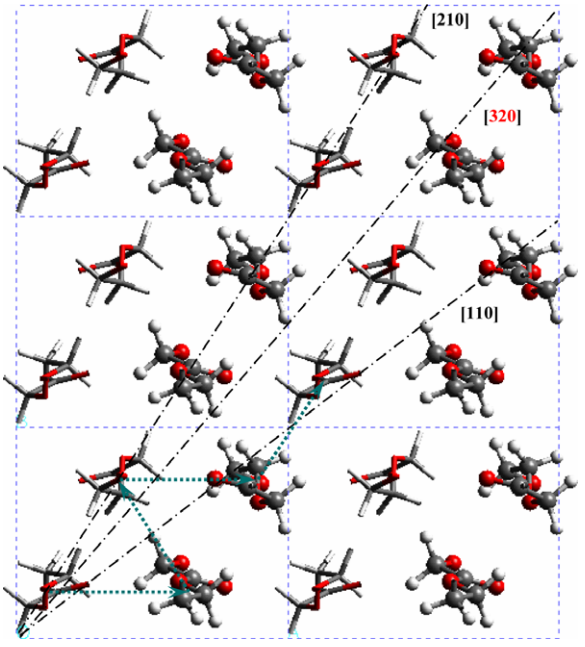

Fig. 15. Two-dimensional representation of the projection onto a 0 0 1 plane of several unit cells of poly(*p*-dioxanone). Distribution of up (sticks) and down (ball and sticks) chains prevents all folds from occurring in the [2 1 0] direction. A mixture of different kinds of folds is required when the growth face differs from {0 1 0}. A possible pattern of folds yielding an average growth normal to the {1 1 0} planes is indicated in green. (For interpretation of the references in color in this figure legend, the reader is referred to the web version of this article.)

the [2 1 0] direction. Thus, adjacent reentry of the folds cannot occur in the [2 1 0] direction exclusively. A combination of different kinds of folds (Fig. 15) may be at play in the observed {1 1 0} and {3 2 0} growth faces.

4. Conclusions

Poly(*p*-dioxanone) crystallizes in an orthorhombic unit cell with space group $P2_12_12_1$ and parameters: $a = 0.970$ nm, $b = 0.751$ nm and c (chain axis) $= 0.650$ nm. The chain periodicity corresponds to a single residue that adopts a TGT$\overline{\text{G}}$ TT conformation according to quantum mechanical calculations performed on small model compounds. The binary screw axis parallel to the chain axis does not correspond to a molecular symmetry but relates neighboring chains arranged along the [1 2 0] direction. These chains have the same up or down orientation, and consequently folding is precluded along this direction.

Lamellar crystals of poly(*p*-dioxanone) are thin and show a lozenge morphology with an acute apex angle that varies depending on the crystallization conditions. The combination of different folds for adjacent reentry can justify the observed {1 1 0} and {3 2 0} growth faces and the difficulty to attain an ordered polyethylene decoration indicative of a regular folding surface.

Poly(*p*-dioxanone) lamellae are degraded by enzymatic attack with esterase activity. This attack takes place on the lateral faces of crystals.

Spherulites with negative birefringence and a ringed texture, the latter indicative of lamellar twisting, can be obtained by evaporation of formic acid solutions. The *a* crystallographic axis of the constitutive lamellae is oriented along the spherulite radius.

Acknowledgements

This research has been supported by the CICYT and FEDER (Grant MAT 2006-02406). We would like to express our gratitude to Dr. Jordi Díaz of the Scientific-Technical Services of UB for the AFM images.

References

[1] Yang KK, Wang XL, Wang YZ. J Macromol Sci Polym Rev 2002;C42(3):373.
[2] Doddi N, Vesfelt C. Wasserman, U.S. Patent 4,052,988, 1977.

[3] Ray JA, Doddi N, Regula D, Williams JA, Melveger A. Surg Gynecol Obstet 1981;153:497.
[4] Jarret TW, Pardalidis NP, Sweetser P, Badlani GH, Smith AD. J Laparoendosc Surg 1995;5:105.
[5] Li XW, Xiao J, Li XY, Xiong CD, Deng XM. Polym Mater Sci Eng 1998;14:20.
[6] Sabino MA, Feijoo JL, Müller AJ. Macromol Chem Phys 2000;38:2436.
[7] Andjelic S, Jamiolkowski D, McDivitt J, Fischer J, Zhou J, Vetrecin R. J Appl Polym Sci 2001;79:742.
[8] Andjelic S, Jamiolkowski D, McDivitt J, Fischer J, Zhou J, Wang Z, et al. J Polym Sci Part B: Polym Phys 2001;39:153.
[9] Andjelic S, Fitz B. J Polym Sci Part B: Polym Phys 2000;38:2436.
[10] Andjelic S, Jamiolkowski D, McDivitt J, Fischer J, Zhou J. J Polym Sci Part B: Polym Phys 2001;39:3073.
[11] Sabino MA, Albuerne J, Müller AJ, Brisson J, Prud'homm RE. Biomacromolecules 2004;5:358.
[12] Sabino MA, Feijoo JL, Müller AJ. Polym Degrad Stab 2001;73:541.
[13] Sabino MA, Sabater L, Ronca G, Müller AJ. Polym Bull 2002;48:291.
[14] Sabino MA, Ronca G, Müller AJ. J Mater Sci 2000;35:5071.
[15] Albuerne J, Márquez L, Müller AJ, Raquez JM, Degée PH, Dubois Ph, et al. Macromolecules 2003;36:1633.
[16] Albuerne J, Márquez L, Müller AJ, Raquez JM, Degée PH, Dubois Ph. Macromol Chem Phys 2005;206:903.
[17] Müller AJ, Albuerne J, Marquez L, Raquez JM, Degée Ph, Dubois Ph, et al. Farad Discuss 2005;128:231.
[18] Furuhashi Y, Nakayama A, Monno T, Kawahara Y, Yamane H, Kimura Y, et al. Macromol Rapid Commun 2004;25:1943.
[19] Casas MT, Gestí S, Puiggalí J. Resúmenes de la XXII Reunión Bienal de la Sociedad Española de Microscopía. 2005, p. 253–4.
[20] Wittmann JC, Lotz B. J Polym Sci Part B: Polym Phys 1985;23:205.
[21] Frisch MJ et al. Gaussian 03, Revision B.02. Pittsburgh (PA): Gaussian Inc.; 2003.
[22] Becke AD. J Chem Phys 1993;98:1372.
[23] Lee C, Yang W, Parr RG. Phys Rev B 1993;37:785.
[24] McLean AD, Chandler GS. J Chem Phys 1980;72:5639.
[25] Cerius^2. Cambridge (UK): Accelrys Inc.
[26] Pouget E, Almontassir A, Casas MT, Puiggalí J. Macromolecules 2003;36:698.
[27] Kanamoto T, Tanaka K. J Polym Sci Part A-2 1971;9:2043.
[28] Furuhashi Y, Iwata T, Sikorski P, Atkins E, Doi Y. Macromolecules 2000;33:9423.
[29] Iwata T, Doi Y. Polym Int 2002;51:852.
[30] Geil PH. Polymer 1963;4:404.
[31] Heber I, Lehman J. Kolloid Z Z Polym 1964;194:7.
[32] Heber I. Kolloid Z Z Polym 1964;200:7.
[33] Hoffman JD, Miller RL. Polymer 1997;38:3151.
[34] Sadler DM. Polymer 1983;24:1401.
[35] Mansfield ML. Polymer 1988;9:755.
[36] Toda A. Polymer 1991;2:71.
[37] Point JJ, Villers D. J Cryst Growth 1991;14:28.
[38] Gan Z, Abe H, Doi Y. Biomacromolecules 2000;1:713.
[39] Gestí S, Casas MT, Puiggalí J. Biomacromolecules 2006;7:799.
[40] Allen FH, Kennard O, Taylor R. Acc Chem Res 1983;16:146.
[41] McCann S, McCann M, Devereux M, McKee V, McMichael P, McCrea JG. Polyhedron 1997;16:4247.
[42] Asakawa M, Brown CL, Menzer S, Raymo FM, Stodart JF, Williams DJ. J Am Chem Soc 1997;119:2614.
[43] Ueda AS, Chatani Y, Tadokoro H. Polym J 1971;2:387.
[44] Liau W, Boyd RH. Macromolecules 1990;23:1531.